To appear in:

Journal of Theoretical and Applied Physics

Online ISSN: 2251-7235 **Print ISSN: 2251-7227**

Received: 07 October 2025
Revised: 14 November 2025
Accepted: 23 April 2026

Accepted Manuscript (Author Version)

DOI: https://doi.org/10.57647/jtap.2026.2005.03

Research Article

Computational Assessment of PbO-Modulated Glass Systems for Advanced Tri-Modular Radiation Shielding

Lucky Makhathini[1,2]*, Sinenhlenhla Fortunate Sihlangu[3], Bonginkosi Vincent Kheswa[4]

[1]Department of Physics and Astronomy, University of the Western Cape, P/B X17, Bellville 7535, South Africa
[2]iThemba Laboratory Accelerator Based Sciences, Tandem Accelerator Mass Spectrometry, 92 Empire Road, Braamfontein, 2017
[3]Academic Development Unit, University of Witwatersrand, South Africa
[4]Department of Physics, University of Johannesburg, 55 Beit Street, Doornfontein, 2028, South Africa

***Corresponding author:** lmakhathini@tlabs.ac.za

ORCID: https://orcid.org/0000-0002-0740-1195

Abstract

This study presents a comprehensive computational investigation of X-ray, γ-ray, and neutron shielding characteristics of six novel glass systems with the composition (75-x)B_2O_3 – 10TeO_2 – 13SrO – 2ZnO – (x)PbO (x = 0, 5, 10, 15, 25, 40 mol%). Using the Phy-X/PSD software, key shielding parameters—including the mass attenuation coefficient (MAC), linear attenuation coefficient (LAC), half-value layer (HVL), tenth-value layer (TVL), mean free path (MFP), effective atomic number ($Z_e$ff), and effective electron density ($N_e$ff)—were determined across photon energies from 0.015 to 15 MeV. The results reveal that increasing PbO concentration significantly enhances photon attenuation, particularly within the photoelectric absorption region below 0.3 MeV. A pronounced peak near 0.1 MeV was observed in MAC, HVL, TVL, MFP, $Z_e$ff, and $N_e$ff, corresponding to the K-absorption edge of lead (0.088 MeV). Among the investigated samples, the glass containing 40 mol% PbO (S6) exhibited the highest MAC and $Z_e$ff, as well as the lowest HVL, TVL, and MFP, indicating superior radiation shielding efficiency. These findings confirm the potential of PbO-modified telluro-borate glasses as effective alternatives for transparent shielding applications in radiological and nuclear environments.

Keywords: Radiation shielding; PbO-borate glass; Phy-X/PSD; Half-value layer; Tenth value layer; Linear attenuation coefficient; Effective atomic number; Effective electron density; Y-ray attenuation

1. Introduction

X-rays are a form of ionizing electromagnetic (EM) radiation, with energies ranging from a few electron volts to hundreds of keV. They are widely used in various industrial applications, including computed tomography scans, dental imaging, and maintenance of power plant piping [1-2]. In contrast, gamma (γ) radiation consists of higher-energy ionizing EM waves, typically emitted during nuclear de-excitation events at several MeV. Both research facilities and industries leverage γ-rays for applications such as γ-spectroscopy and the sterilization of surgical instruments. Neutrons, another type of ionizing subatomic particle, are common in nuclear reactor environments, produced through nuclear fission. Their applications include electrical power generation, neutron diffraction, and neutron tomography. Despite their usefulness, X-rays, γ-rays, and neutrons present significant health hazards to personnel in these fields if proper shielding is not in place [1].
A variety of materials have been developed to shield against X-rays, γ-rays, and neutrons. Traditionally, lead plates have been used for photon shielding, while concrete has been employed for both photons and neutrons. However, these materials have notable drawbacks, such as lead's toxicity and the challenges associated with the weight and maintenance of both lead and concrete [1-3]. Furthermore, prolonged exposure to nuclear radiation can cause heating in concrete, leading to structural integrity issues such as cracking and potential radiation leakage [2,4,5]. The opacity of lead and concrete also complicates real-time observation, hindering the timely detection of irregularities where visual monitoring is crucial [3].

In light of these challenges, there is considerable global research interest in identifying optimal heavy metal oxide glass materials, either lead-free or with minimal lead content, for effective shielding against ionizing electromagnetic radiation [6-36]. Recent studies have investigated various glass compositions, yielding promising results. For example, research on bismuth-borate glass doped with rare-earth ions has shown enhanced X-ray shielding efficacy, with Sm^{3+}-doped glass outperforming both Nd^{3+} and Ce^{3+} counterparts [23]. Computational studies on $Bi_2O_3 – B_2O_3 – TeO_2 – TiO_2$ glass indicate strong potential for X-ray shielding, particularly in the dental diagnostic energy range, suggesting its applicability in protective mask fabrication during oral cavity irradiation [19 -29]. Similarly, investigations into $Li_2O – B_2O_3 – MgO – Er_2O_3$ glass, doped with Sm_2O_3, have demonstrated improved photon shielding capabilities with increased Sm_2O_3 content. Research on $La_2O_3 – CaO – B2O_3 – SiO_3$ glass has revealed enhanced X-ray shielding efficiency with higher concentrations of La_2O_3 [25].

Recent studies have also explored the photon shielding properties of borate glass compositions, noting enhancements from the addition of various components, including $Cr2O_3$, TeO_2, Gd_2O_3, WO_3, TeO_2/MoO_3, and CeO_2 [27-33]. In another approach [43], bulk metallic glass samples were analyzed, revealing that $T_{i41.9}Zr_{36.3}V_{12.1}Cu_{6.3}Be_{3.4}$, characterized by the lowest Ti and highest Zr content, exhibited superior neutron shielding capabilities among the samples studied. One investigation assessed the impact of Ag content on the fast neutron shielding properties of glass samples, finding improvements

with increased Ag concentrations [37]. Additionally, computational analyses of $Li2B_4O_7$ – $Bi2O_3$ – ZrO_4 – $CaWO_4$ highlighted improved neutron shielding efficiency correlating with higher B2O3 concentrations [40-46].

In a recent study [30], six novel glass compositions were synthesized, represented by the formula (75 − x)$B2O_3$– 10TeO_2 – 13SrO – 2ZnO – (x)PbO, where x varied from 0 to 40 mol%. Despite their innovative nature, the radiation shielding properties of these materials remain unexplored. This study aims to conduct a thorough investigation of the X-ray, γ-ray, and neutron shielding capabilities of these novel glass systems. Specifically, computational assessments will evaluate key parameters, including the mass attenuation coefficient (MAC), linear attenuation coefficient (LAC), half-value layer (HVL), tenth-value layer (TVL), mean free path (MFP), effective atomic number (Z_{eff}), and effective electron density (N_{eff}).

2. Computational tools and theoretical framework

Analysis of the X-ray, γ-ray, and neutron shielding properties of six innovative glass samples, detailed in Table 1, was conducted using Phy-X/PSD software. The selection of Phy-X/PSD as the primary analytical tool for radiation shielding research is justified by its superior efficiency, comprehensive parameter output, and its ability to bridge the gap between theoretical physics and practical material engineering. While traditional databases like NIST XCOM [46,47] provide foundational data, they often require significant manual post-processing to derive engineering-relevant metrics. Phy-X/PSD eliminates this burden by offering an integrated platform that calculates a vast array of shielding and dosimetry parameters simultaneously, making it an indispensable asset for modern materials science. Phy-X/PSD operates on a remote server equipped with an Intel(R) Core(TM) i7-2600 CPU @ 3.40 GHz processor and 1 GB of installed memory, running on the Ubuntu 14.04.3 LTS operating system [44,45, 41]. Across the energy range of 15 keV to 15000 keV, Phy-X/PSD was employed to compute MAC, LAC, HVL, TVL, MFP, Z_{eff} and N_{eff}. The theoretical underpinnings of these radiation shielding calculations are elucidated below.

Table 1:Chemical content (mol%) and density of glass samples [37]

Code	B_2O_3	TeO_2	SrO	ZnO	PbO	ρ (g/cm^3)
S1	75	10	13	2	0	3.09
S2	70	10	13	2	5	3.29
S3	65	10	13	2	10	3.48
S4	60	10	13	2	15	3.70
S5	50	10	13	2	25	4.05
S6	35	10	13	2	40	4.72

The linear attenuation coefficient (μ)serves as a metric for assessing the probability of photon interaction with radiation shielding material, encompassing contributions from the photoelectric effect, Compton scattering, and pair production. This coefficient's variation with photon energy (E) and absorber atomic number (Z) mirrors the dependencies of these processes on E and Z. The linear attenuation coefficient (LAC) is governed by the Beer-Lambert law, linking it to both photon intensity and absorber thickness (x), as follows [39]

$$I(x) = I_0 e^{(-\mu x)}, \quad (1)$$

where I_0 and $I(x)$ represent the photon intensities before and after traversing an absorber with thickness x, respectively. The effectiveness of attenuating x-rays and γ-rays is directly linked to the value of μ. A higher μ value implies enhanced material capability in attenuating these forms of radiation.

Similarly, the mass attenuation coefficient (MAC) provides a measure of the probability of attenuating γ-rays within an absorber material. However, in contrast to the linear attenuation coefficient, it remains independent of material density. Instead, the mass attenuation coefficient is solely determined by the photon energy and the absorber's atomic number. It is calculated according to [39]

$$MAC = \sum w_i \left(\frac{\mu}{\rho}\right)_i, \quad (2)$$

where w_i represents the weight of the i^{th} constituent element in the absorber.

The half-value layer (HVL) and tenth-value layer (TVL) stand as crucial parameters in explicating the shielding efficacy against X-ray and γ-ray radiation. Analogous to the temporal concept of half-life in nuclear decay phenomena, the HVL denotes the material thickness requisite to halve the initial photon intensity. Likewise, the TVL signifies the absorber thickness needed to diminish photon intensity by a factor of ten. A reduction in both HVL and TVL values indicates enhanced efficiency in radiation attenuation. These are computed from the linear attenuation coefficient as follows [45]

$$HVL = \frac{0.693}{\mu} \quad (3)$$

and

$$TVL = \frac{ln10}{\mu}. \quad (4)$$

Moreover, the mean-free path (MFP) represents the mean distance traversed by a photon within an absorber before encountering either the photoelectric effect, Compton scattering, or pair production. Materials exhibiting lower MFP values are regarded as more proficient in shielding X-ray and γ rays compared to those with higher MFP values. It is given by [45]

$$MFP = 1.44HVL \quad (5)$$

The effective atomic number (Z_{eff}) is derived from the linear attenuation coefficient and the density of an absorber, as specified in the expression below [45].

$$Z_{eff} = \frac{\sum_j f_j A_j \left(\frac{\mu}{\rho}\right)_j}{\sum_j \frac{f_j A_j}{Z_j} \left(\frac{\mu}{\rho}\right)_j} \quad (6)$$

where f_j, A_j, and Z_j denote the mole fraction, atomic weight, and atomic number of each constituent element within the sample, respectively. Higher values of Z_{eff} correspond to heightened radiation shielding efficacy exhibited by the material.

The effective electron density for each glass sample is calculated from its mass attenuation coefficient using the formula below:

$$N_{eff} = \frac{MAC}{\sigma_e} \quad (7)$$

where σ_e represents the total electronic cross-section, which is determined using the following equation:

$$\sigma_e = \frac{\frac{1}{N_A \sum_i (w_i/A_i)} MAC}{Z_{eff}} \quad (8)$$

In this context, A_i denotes the atomic weight of the ith element in the sample, and w_i represents its weight fraction. Additionally, N_A refers to Avogadro's number.

3. Results and discussions

Figure 1 illustrates the Mass Attenuation Coefficient (MAC) profiles for the six glass samples under investigation. It is observed that Sample 6 (S6) exhibits the highest MAC values, while Sample 1 (S1) displays the lowest. The MAC values demonstrate a clear upward trend with increasing PbO concentration, a finding that is in high agreement with established literature [40, 41, 43]. This correlation confirms that the systematic addition of PbO significantly enhances the radiation shielding properties of the glass matrix.

The maximum MAC values for all compositions were recorded at the lowest energy point of 0.015 MeV. At this level, S1 (0 mol% PbO) yielded a MAC of 12.91 cm²/g, whereas S6

(40 mol% PbO) reached a peak value of 71.14 cm²/g. Furthermore, Sample 2 (S2), which contains 5 mol% PbO, demonstrated a Linear Attenuation Coefficient (LAC) of 24.91 cm^{-1}. The inclusion of PbO in the glass samples results in a significant increase in MAC values, particularly at lower energy intervals. These energies fall strictly within the photoelectric absorption regime, which is the primary interaction mechanism for gamma-ray attenuation in this energy range [41, 42].

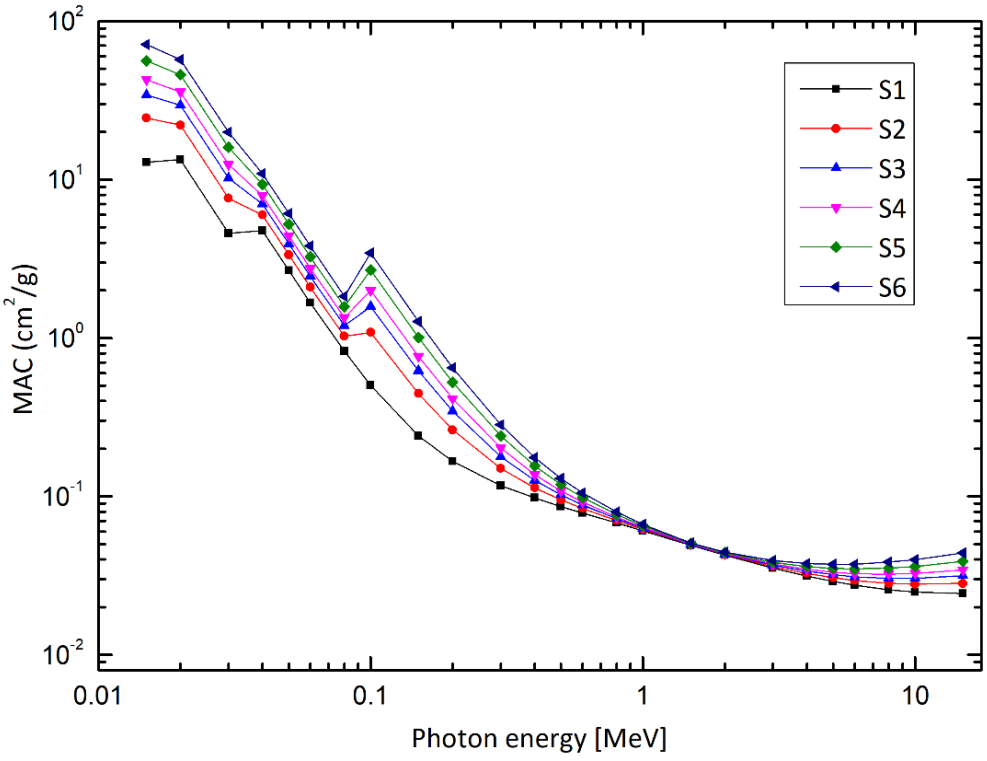

Figure 1: Mass Attenuation Coefficient as a function of energy between 0,0015 MeV to 15 MeV.

Increasing the PbO concentration in the (75-x)B_2O_3 – 10TeO_2 – 13SrO – 2ZnO – (x)PbO glass samples causes a spike in the MAC values at 0.1 MeV. A PbO concentration of 5%, 10%, 15%, 25% and 40% increases MAC by a factor of 2.16, 3.15, 3.99, 5.35 and 6.85 respectively at 0.1 MeV. This spike at 0.1 MeV is due to the K absorption edge of Pb at 0.088 MeV. This result is also consistent with Ref. [48] and [49]. A spike (or sudden peak) close to 0.1 MeV is seen in the MAC curve of (x)PbO – (100-x)TeO_2, x = 10, 20, 30 mol% glass compositions in ref. [48]. Ref. [49] reports peaks at 0.8 MeV in the MAC curves of (100-x)B_2O_3-(x)PbO where x = 20, 30, 40, 50 and 60 mol %, (100-x)SiO_2-(x)PbO, where x= 32, 42, 52 and 62 mol% and (100 – x)GeO_2-(x)PbO, where x=0, 10, 20 mol% glass compositions.

At photon energies of $0.8\ \mathrm{MeV} \leq E_p \leq 3.0\ \mathrm{MeV}$, the LAC values are negligibly affected by the increase in PbO concentration. This energy range is the Compton scattering mode and

ref. [40] also reports that (x)PbO – (100-x)TeO_2, x = 10, 20, 30 mol% glass samples had MAC values that were almost unaffected by the increase in PbO concentration.

Figure 2 and Figure 3 show the half-value layer and tenth-value layer, respectively. S6 has the lowest HVL and TVL values. S1 has the highest HVL and TVL values. The addition of PbO reduces the HVL and TVL values thus increasing shielding capability of the material. The TVL values of samples S2 – S6 increase at energies, 0.01 MeV to 0.08 MeV. There is a slight decline in TVL and HVL values for samples S2 – S6 at 0.1 MeV. Sample 6, which has the highest concentration of PbO shows the greatest decline in the TVL values from 0.08 MeV to 0.1 MeV.

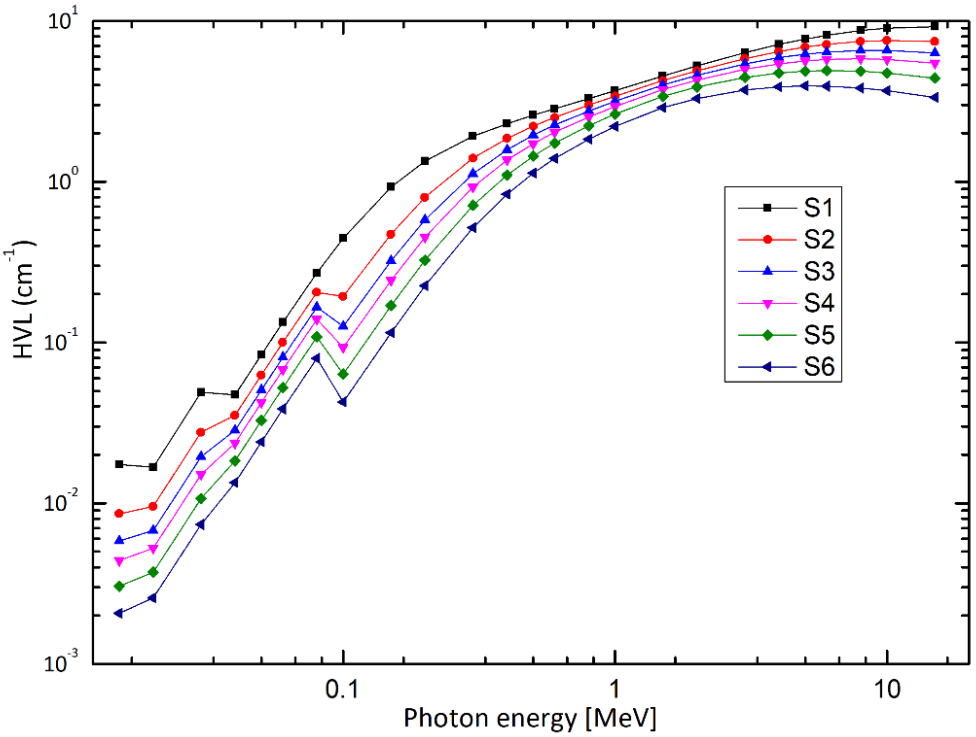

Figure 2: Half-value layer as a function of Energy for all grass ssamples

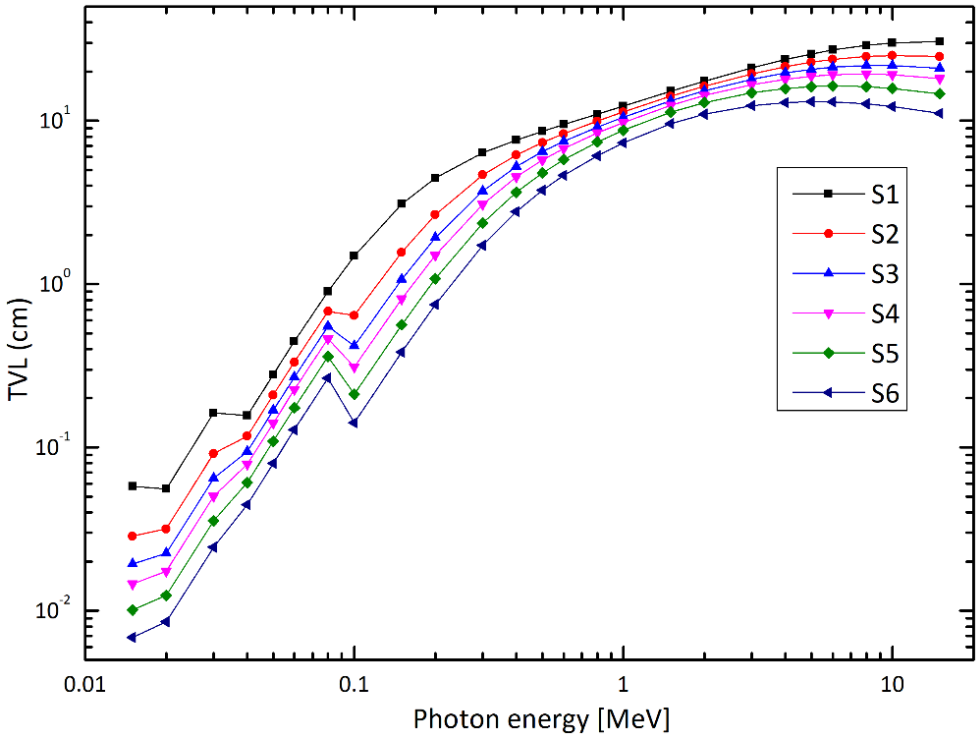

Figure 3:Tenth value layer as a function of energy for all grall samples

Figure 4 shows the mean free path of the six samples. Sample 1 has the highest mean free path at all energy levels and Sample 6 has the lowest mean free path at all energy levels. The addition of PbO in the samples S2 – S6 decreases the values of MFP. This trend can be attributed to the density of the samples. The MFP is inversely proportional to the density of the sample [49]. Equation 3 and 5 show that MFP is also inversely proportional to the LAC and it is shown in *Figure 1* that LAC increases with increasing PbO concentration. Since the LAC is increasing with increasing PbO concentration then the MFP will decrease with increasing PbO concentration. Like Figure 3, there is a decline in the MFP values of S2 – S6 at 0.1 MeV. The biggest decline at 0.1 MeV is seen in S6, which contains the largest concentration of PbO.

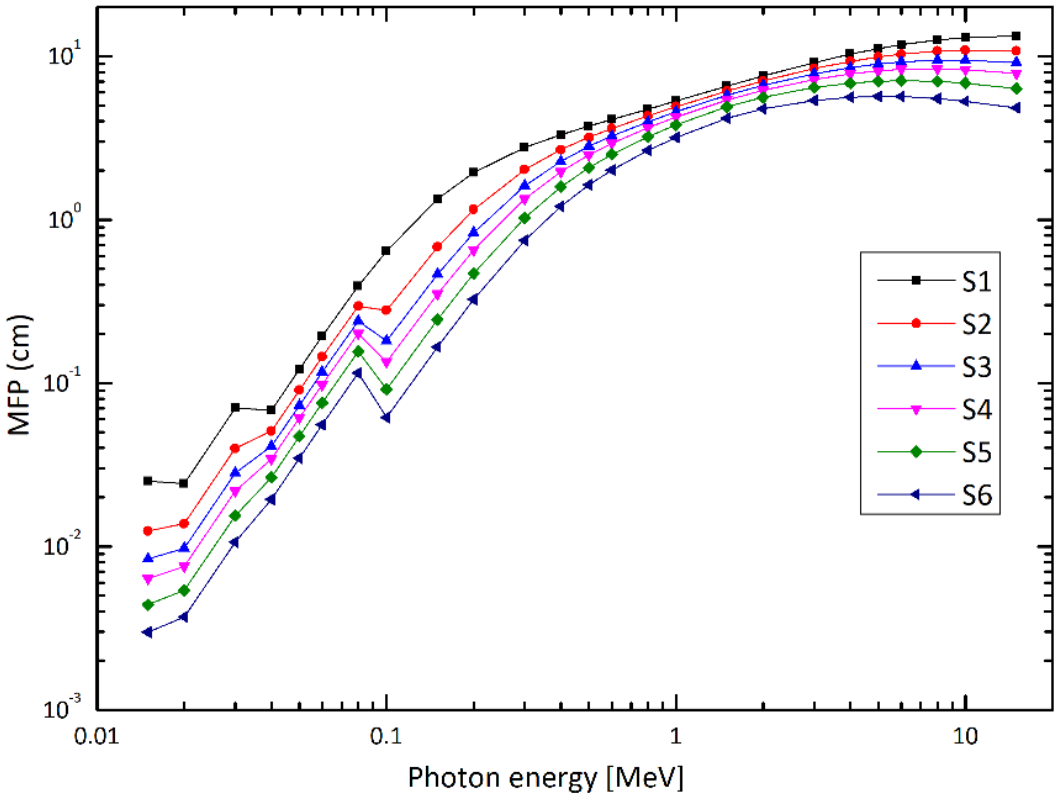

Figure 4: Mean free path as a function of Energy for all gralss samples.

Figure 5(b) shows the Z_{eff} for the six samples. The values of Z_{eff} increase with increasing PbO concentration; the same trend can be seen in ref [41,43,47] for lead borate samples. Z_{eff} values for S2-S6 peak at 0.1 MeV and are 37.88, 47.98, 54.78, 63.29, 70.30 for S2 – S6. The lowest values of Z_{eff} are at 1.5 MeV for all six samples, which are 9.07, 10.38, 11.71, 13.13, 16.29 and 21.9.

Figure 5(a) shows the variation of effective electron density as a function of photon energy for six different samples labelled S1–S6. The photon energy range extends from 0.01 MeV to 10 MeV on a logarithmic scale, while the effective electron density ranges from about 4 × 10^{23} to 1.4 × 10^{24} electrons/cm³. At low photon energies (below 0.1 MeV), all samples exhibit relatively high effective electron densities, indicating strong photon–electron interactions dominated by the photoelectric effect. As photon energy increases, N_{eff} decreases sharply, reaching a minimum around 1 MeV, where Compton scattering becomes the dominant interaction process. Beyond this region, N_{eff} gradually increases again at higher energies due to the onset of pair production processes.

Among the samples, S4 and S3 consistently show the highest N_{eff} values across most energies, while S1 exhibits the lowest. The overall trend is similar for all materials, reflecting that their elemental compositions influence electron density but follow the same general photon–matter interaction behaviour. This indicates that although the samples differ in composition or structure, they share similar radiation response characteristics across the studied energy range.

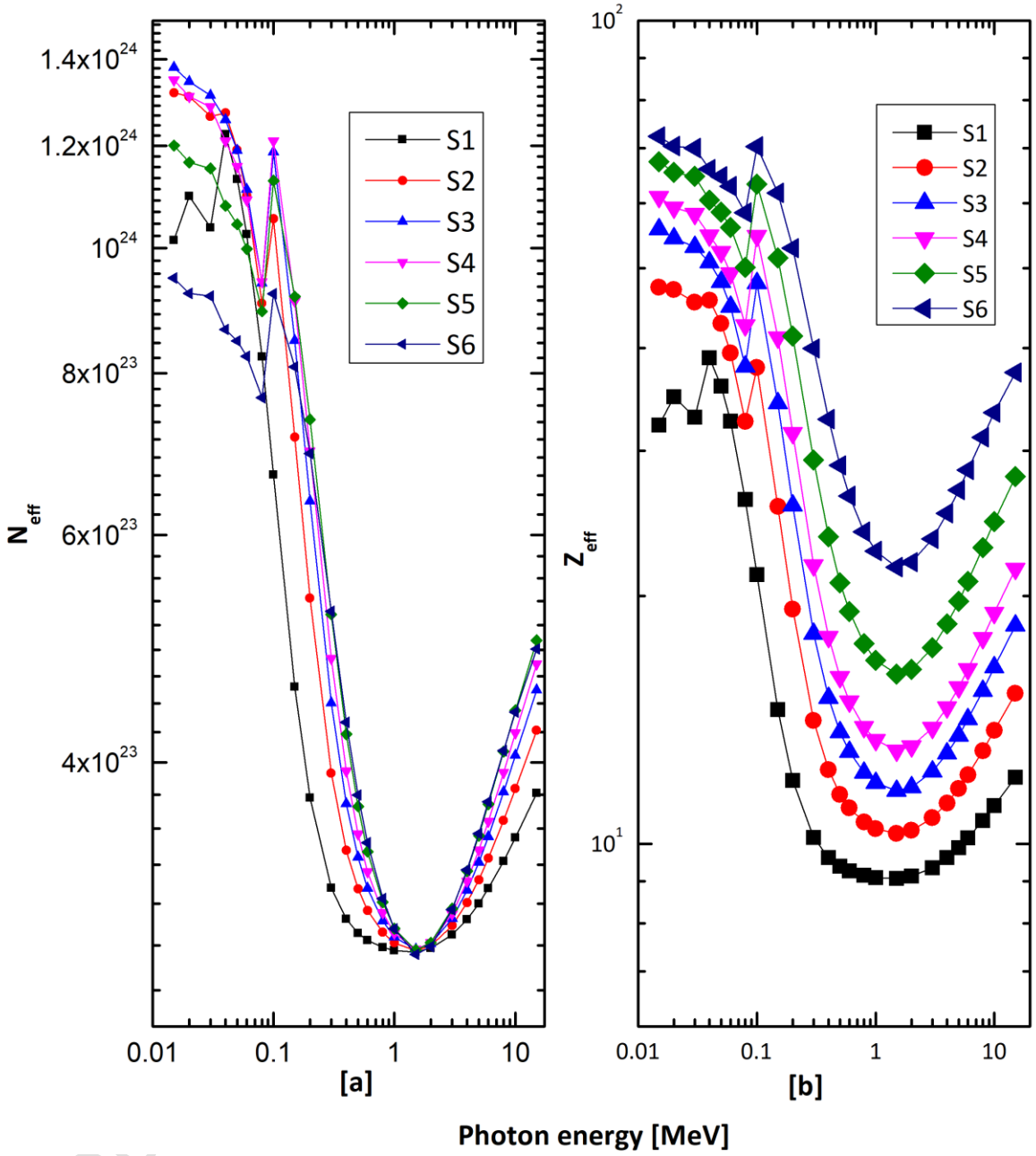

Figure 5: N_{eff} and Z_{eff} as a function of energy for all glass samples .

The utilization of Lead Oxide (PbO) in radiation shielding presents a classic engineering paradox where high physical performance must be reconciled with significant biological and structural liabilities. From a performance standpoint, PbO is unrivalled in its ability to increase a material's Effective Atomic Number (Zeff) and density, directly enhancing its photon-stopping power. However, this efficiency is counterbalanced by the environmental toxicity of lead, which necessitates stringent and costly regulatory compliance during both the manufacturing and disposal phases. Furthermore, high PbO concentrations often lead to mechanical fragility, as lead ions act as network modifiers that can disrupt the structural

integrity of glass or polymer matrices, resulting in reduced hardness and increased susceptibility to scratches.

4. Conclusion

In conclusion, the computational investigation into the (75−x)B2O3–10TeO_2–13SrO–2ZnO–(x)PbO (x=0 to 40 mol%) glass systems reveals that the systematic incorporation of PbO significantly enhances radiation shielding performance across X-ray, γ-ray, and neutron energy spectra. Analysis using the Phy-X/PSD platform across an energy range of 0.015 to 15 MeV demonstrates that increasing PbO concentration leads to a consistent rise in the mass attenuation coefficient (MAC), linear attenuation coefficient (LAC), effective atomic number (Zeff), and effective electron density (Neff). Simultaneously, the substitution of B_2O_3 with PbO markedly reduces the half-value layer (HVL), tenth-value layer (TVL), and mean free path (MFP), indicating superior attenuation efficiency. Among the studied samples, the glass containing 40 mol% PbO (S6) exhibited the highest shielding proficiency, recording a maximum MAC of 71.14 cm2/g at 0.015 MeV and a peak Zeff of 70.30.

A distinctive performance peak was observed across all parameters near 0.1 MeV, which corresponds to the K-absorption edge of lead at 0.088 MeV, confirming the dominant influence of Pb-based interactions in the low-energy photoelectric absorption region. While the impact of PbO becomes negligible in the Compton scattering region (0.8 MeV to 3.0 MeV), the N_{eff} values were observed to rise again at higher energies due to the onset of pair production. Despite the inherent engineering paradox regarding lead toxicity and potential mechanical fragility at high concentrations, these results underscore the potential of PbO-modified telluro-borate glasses as efficient, tunable, and transparent alternatives to traditional shielding materials like concrete and lead plates for use in medical radiology and nuclear facilities

Author contributions: The authors did all simulations and compiled the manuscript.

Conflict of interest: The authors declare that there is no conflict of interest to this work.

Data availability statement: All data presented in this article are available on request.

Ethical approval: This research work does not involve humans or animals.

References

[1] Klein RC, Weilandics C. Potential health hazards from lead shielding. Am. Ind. Hyg. Assoc J. 1996; 57(12):1124-6. doi: 10.1080/15428119691014215.

[2] M. I. Sayyed *et al.*, “Optical, physical, mechanical, structural, and radiation shielding investigations of B2O3–TeO2-GeO2-MgO-PbO for ionizing protection and optical transmission application,” *Opt Mater (Amst)*, vol. 154, p. 115807, Aug. 2024, doi: 10.1016/J.OPTMAT.2024.115807.

[3] ,Tekin, H.O., et al.. Radiation shielding properties of some glass systems: A review. Journal of Non-Crystalline Solids. 2019; 512:1-15.

[4] Sayyed MI, Kaky KM, Anaee RA. Chromium ions effects on Sb_2O_3-PbO-GeO_2 glass properties for radiation protection. J. Theor. Appl. Phys. 2023; 17(5):172355(1-6). https://dx.doi.org/10.57647/j.jtap.2023.1705.55

[5] Scuderi GJ, Brusovanik GV, Campbell DR, Henry RP, Kwon B, Vaccaro AR. Evaluation of non–lead-based protective radiological material in spinal surgery. Spine J. 2006;6:577. https://doi.org/10.1016/j.spinee.2005.09.010

[6] Sayyed MI, Tekin HO, Kılıcoglu O, Agar O, Zaid MHM. Shielding features of concrete types containing sepiolite mineral: comprehensive study on experimental, XCOM and MCNPX results. Results Phys. 2018;11:40. https://doi.org/10.1016/j.rinp.2018.08.029

[7] Akkurt I, Akyildirim H, Mavi B, Kilincarslan S, Basyigit C. Gamma-ray shielding properties of concrete including barite at different energies. Prog. Nucl. Energy 2010;52:620.
https://doi.org/10.1016/j.pnucene.2010.04.006

[8] Hosseini, S.G., et al.. Investigation of gamma-ray shielding parameters of some borate glasses containing heavy metal oxides. Journal of Non-Crystalline Solids. 2017; 471:1-9.

[9] Tekin HO, ALMisned G, Zakaly HMH, Zamil A, Khoucheich D, Bilal G, et al. Gamma, neutron, and heavy charged ion shielding properties of Er^{3+}-doped and Sm^{3+}-doped zinc borate glasses. Open Chem. 2022; 20:130-45. doi: 10.1515/chem-2022-0128.

[10] M. H. A. Mhareb *et al.*, “Improving structural, optical, and ionizing absorption features of G-T-B glass system by doping different concentration of Sm2O3,” *Ceram Int*, vol. 51, no. 3, pp. 3809–3819, Jan. 2025, doi:10.1016/J.CERAMINT.2024.11.356.

[11] Waly ESA, Fusco MA, Bourham MA. Gamma-ray mass attenuation coefficient and half value layer factor of some oxide glass shielding materials. Ann. Nucl. Energy 2016;96:26 – 30.
doi: 10.1016/j.anucene.2016.05.028

[12] ALMisned G, Elshami W, Issa S, Susoy G, Zakaly H, Algethami M, et al. Enhancement of Gamma-ray Shielding Properties in Cobalt-Doped Heavy Metal Borate Glasses: The Role of Lanthanum Oxide Reinforcement. Materials 2021;14:7703. doi: 10.3390/ma14247703.

[13] Kaur S, Singh K. Investigation of lead borate glasses doped with aluminium oxide as gamma ray shielding materials. Ann. Nucl. Energy 2014;63:350-4. doi: 10.1016/j.anucene.2013.08.012.

[14] Akkurt I, Malidarre R, Kavas T. Monte Carlo simulation of radiation shielding properties of the glass system containing Bi_2O_3. Eur. Phys. J Plus 2021;136:264. doi: 10.1140/epjp/s13360-021-01260-y.

[15] Sayyed M, Elbashir B, Tekin H, Altunsoy E, Gaikwad D. Radiation shielding properties of pentaternary borate glasses using MCNPX code. J Phys. Chem. Solids 2018;121:17–21.
doi: 10.1016/j.jpcs.2018.05.009.

[16] Kurudirek M, Ozdemir Y, Simsek O, Durak R, Comparison of some lead and non-lead based glass systems, standard shielding concretes and commercial window glasses in terms of shielding parameters in the energy region of 1keV – 100 GeV: A comparative study. Journal of Nuclear Materials 2010; 407:110-115. doi: 10.1016/j.jnucmat.2010.10.007

[17] Sopapan P, Laopaiboon J, Jaiboon O, Yenchai C, Laopaiboon R. Feasibility study of recycled CRT glass on elastic and radiation shielding properties used as X-ray and gamma-ray shielding materials. Prog. Nucl. Energy 2020;119:103149.

[18] Sayyed M, Çelikbilek Ersundu M, Ersundu AE, Lakshminarayana G, Kostka P. Investigation of radiation shielding properties for $MeOPbCl_2 – TeO_2$ ($MeO = Bi_2O_3$, MoO_3, Sb_2O_3, WO_3, ZnO) glasses. Radiat Phys Chem. 2018;144:419-25. doi: 10.1016/j.radphyschem.2017.10.005.

[19] Kurudirek, M.. Effective atomic numbers of some glass systems: A comparative study. Radiation Physics and Chemistry. 2014; 102:45-50.

[20] S. E. layan Alawaideh *et al.*, “Effect of different metal oxides on the Radiation shielding features of borate glasses,” *Radiation Physics and Chemistry*, vol. 220, p. 111720, Jul. 2024, doi: 10.1016/J.RADPHYSCHEM.2024.111720.

[21] M. R. Ahmed *et al.*, “Physical, thermal properties, FTIR and Raman spectroscopies as well as γ-ray attenuation capacity of borate glasses doped with Mn2+ ions: Role of CaO/Al2O3 substitution,” *Opt Mater (Amst)*, vol. 158, p. 116461, Jan. 2025, doi: 10.1016/J.OPTMAT.2024.116461.

[22] M. I. Sayyed, M. H. A. Mhareb, R. I. Mahdi, A. J. Kadhim, K. M. Kaky, and M. K. Hamad, “Design, fabrication, and features investigations of high concentration of Yttrium

Oxide doped germanate tellurate borate glass system for optical and radiation shielding application," *Ceram Int*, vol. 50, no. 24, pp. 54490–54497, Dec. 2024, doi:10.1016/J.CERAMINT.2024.10.305.

[23] Kaewkhao J, Pokaipisit A, Limsuwan P. Study on borate glass system containing with Bi_2O_3 and BaO for gamma-rays shielding materials: Comparison with PbO. J Nucl Mater. 2010;399(1):38–40.
doi: 10.1016/j.jnucmat.2009.12.020.

[24] Chanthima N, Kaewkhao J, Limkitjaroenporn P, Tuscharoen S, Kothan S, Tungjai M, et al. Development of BaO – ZnO – B_2O_3 glasses as a radiation shielding material. Radiat Phys Chem. 2017;137: 72-7. doi: 10.1016/j.radphyschem.2016.03.015.

[25] Kheswa BV. X-ray shielding properties of bismuth-borate glass doped with rare-earth ions, Open Chem J. 2023;21:20220345. https://doi.org/10.1515/chem-2022-0345

[26] Al-Hadeethi Y, Sayyed MI, Mohammed H, Rimondini L. X-ray photons attenuation characteristics for two tellurite based glass systems at dental diagnostic energies. Ceram Int. 2020;46:251-257.
https://doi.org/10.1016/j.ceramint.2019.08.258

[27] Mhareb MHA. Physical, optical and shielding features of Li_2O – B_2O_3 – MgO – Er_2O_3 glasses co-doped of Sm_2O_3. Appl Phys A. 2020;126:71. doi: 10.1007/s00339-019-3262-9.

[28] Kaewjaeng S, Kothan S, Chaiphaksa W, Chanthima N, Rajaramakrishna R, Kim H, et al. High transparency La_2O_3 – $CaOB_2O_3$ – SiO_2 glass for diagnosis X-rays shielding material application. Radiat Phys Chem. 2019;160:41-7. doi: 10.1016/j.radphyschem.2019.03.018.

[29] Aktas B, Yalcin S, Dogru K, Uzunoglu Z, Yilmaz D. Structural and radiation shielding properties of chromium oxide doped borosilicate glass. Radiat. Phys. Chem. 2019;156:144-149.
https://doi.org/10.1016/j.radphyschem.2018.11.102

[30] Aktas B, Acikgoz A, Yilmaz D, Yalcin S, Dogru K, Yorulmaz N. The role of TeO_2 insertion on the radiation shielding, structural and physical properties of borosilicate glasses. J. Nucl. Mater. 2022; 563:153619. https://doi.org/10.1016/j.jnucmat.2022.153619

[31] Fidan M, Acikgoz A, Demircan G, Yilmaz D, Aktas B. Optical, structural, physical, and nuclear shielding properties, and albedo parameters of TeO_2 – BaO – PbO – V_2O_5 glasses. J. Phys.Chem. Solids 2022;163:110543. https://doi.org/10.1016/j.jpcs.2021.110543

[32] Solak BB, Aktas B, Yilmaz D, Kalecik S, Yalcin S, Acikgoz A, Demircan G, Exploring the radiation shielding properties of B_2O_3-PbO-TeO_2-CeO_2-WO_3 glasses: A comprehensive study on structural, mechanical, gamma, and neutron attenuation

characteristics. Mater. Chem. Phys. 2024; 312:128672. https://doi.org/10.1016/j.matchemphys.2023.128672

[33] Yorulmaz N, Yasar MM, Acikgoz A, Kavun Y, Demircan G, Kamislioglu M, Aktas B, Ulas EO. Influence of Gd_2O_3 on structural, optical, radiation shielding, and mechanical properties of borate glasses. Opt. Mater. 2024;149:115032. https://doi.org/10.1016/j.optmat.2024.115032

[34] Fidan M, Acikgoz A, Yilmaz D, Demircan G, Kalecik S, Aktas B, Isgor S. Investigation of the structural, mechanical, radiation and neutron shielding properties of the TeO_2-B_2O_3-Li_2O-MoO_3-CuO glass system. J. Alloys Compd. 2024; 976:172981. https://doi.org/10.1016/j.jallcom.2023.172981

[35] Saudi HA, Zakaly HMH, Issa SAM, Tekin HO, Hessien MM, Rammah YS, Henaish AMA. Fabrication, FTIR, physical characteristics and photon shielding efficacy of CeO_2 / sand reinforced borate galsses: Experimental and simulation studies. Radiat. Phys. Chem. 2022;191:109837.
https://doi.org/10.1016/j.radphyschem.2021.109837.

[36][29] Subedi B, Lamichhane TR. Radiation shielding properties of low-density Ti-based bulk metallic glass composites: a computational study. Phys. Scr. 2023;98:035003. https://doi.org/10.1088/1402-4896/acb623

[37] Tuncel N, Akkurt I, Atik I, Malidarre RB, Sayyed MI. Neutron-gamma shielding properties of chalcogenide glasses. Radiat. Phys. Chem. 2024;218:111582. https://doi.org/10.1016/j.radphyschem.2024.111582

[38] Aygün B, Yorgun NY, Sayyed MI, Karabulut A. Li2B4O7–$Bi2O_3$–ZrO4–$CaWO_4$ glass system for neutron protection in neutron applications. Prog. Nucl. Energy 2023;162:104751.
https://doi.org/10.1016/j.pnucene.2023.104751

[39] M. I. Sayyed, M. H. A. Mhareb, K. M. Kaky, and M. K. Hamad, “Structural, mechanical, and radation shielding properties of B2O3–Na2O–PbO–Fe2O3 glass system,” *Radiation Physics and Chemistry*, vol. 222, p. 111848, Sep. 2024, doi: 10.1016/J.RADPHYSCHEM.2024.111848.

[40] K. M. Kaky, M. I. Sayyed, K. A. Mahmoud, M. H. A. Mhareb, S. Biradar, and A. J. Kadhim, “A comprehesive I vestigation on lanthanum ions doped borate-tellurite-germinate glass for radiation shielding and optical application,” *Progress in Nuclear Energy*, vol. 176, p. 105402, Nov. 2024, doi: 10.1016/J.PNUCENE.2024.105402.

[41] H. Al-Ghamdi *et al.*, “Impact of TiO 2-Doped Bismuth-Boro-Tellurite Glasses: Fabrication, Physical and Optical Properties, and γ-Ray Protection Competence for Optical and Radiation Shielding Applications-tellurite glasses · XRD · molar refractivity · MAC · Phy-X/PSD · γ-ray,” *J Electron Mater*, vol. 54, pp. 1432–1443, 1234, doi: 10.1007/s11664-024-11616-6.

[42] R. I. Mahdi, M. Y. Hanfi, M. H. A. Mhareb, M. I. Sayyed, A. J. Kadhim, and K. M. Kaky, “Transparent heavy metal glass-ceramics reinforced with nano-PbO for next-generation X- and γ-ray shielding applications,” *Mater Res Bull*, vol. 195, p. 113808, Mar. 2026, doi: 10.1016/J.MATERRESBULL.2025.113808.

[43] Thabit HA, Es-soufi H, Ismail AK, Bafaqeer A, Sayyed MI. Preparation, structural characterization, and photoluminescence of Pb^{2+} ions doped telluro-borate glass-ceramics. Opt. Quantum Electron. 2024; 56:656. https://doi.org/10.1007/s11082-023-06232-3

[44] https://phy-x.net/PSD.

[45] Sakar E, Ozpolat O, Alım B, Sayyed M, Kurudirek M. Phy-X/PSD: Development of a user-friendly online software for calculation of parameters relevant to radiation shielding and dosimetry. Radiat Phys Chem. 2020;166:108496. doi: 10.1016/j.radphyschem.2019.108496.

[46] https://physics.nist.gov/PhysRefData/Xcom/html/xcom1.html

[47] El-Mallawany, R.. Tellurite glasses handbook: Physical properties and data. Springer. 2011; :1-500.

[48] Alalawi A, Buriahi M.S, Sayyed M.I, Akyildirim H, Arslan H, Zaid M.H.M, Influence of lead and zinc oxides on the radiation shielding properties of tellurite glass systems. Ceramics International.2020;46:17300-17306.https://doi.org/10.1016/j.ceramint.2020.04.017

[49] El-Mallawany R, Sayyed M.I, Dong M.G, Rammah Y.S, Simulation of radiation shielding properties of glasses contain PbO. Radiat. Phys. Chem. 2018;151:239-252 https://doi.org/10.1016/j.radphyschem.2018.06.035